



ELSEVIER

Available online at [www.sciencedirect.com](http://www.sciencedirect.com)

SCIENCE @ DIRECT®

Journal of Contaminant Hydrology 73 (2004) 39–63

JOURNAL OF

Contaminant  
Hydrology

[www.elsevier.com/locate/jconhyd](http://www.elsevier.com/locate/jconhyd)

## Infiltration of PCE in a system containing spatial wettability variations

Denis M. O'Carroll<sup>a,1</sup>, Scott A. Bradford<sup>b,2</sup>, Linda M. Abriola<sup>c,\*</sup>

<sup>a</sup>Department of Civil and Environmental Engineering, University of Michigan, 181 EWRE, 1351 Beal Avenue, Ann Arbor, MI 48109-2125, USA

<sup>b</sup>George E. Brown, Jr., Salinity Laboratory, U.S. Department of Agriculture, Agricultural Research Service, 450 Big Springs Road, Riverside, CA 92507, USA

<sup>c</sup>School of Engineering, Tufts University, 105 Anderson Hall, 200 College Avenue, Medford, MA 02155, USA

Received 23 April 2002; received in revised form 1 December 2003; accepted 10 December 2003

### Abstract

A two-dimensional infiltration experiment was conducted to investigate and quantify the effect of spatial wettability variations on DNAPL migration and entrapment in saturated sands. Experimental observations of tetrachloroethylene (PCE) infiltration showed that organic-wet sand lenses acted as very effective capillary barriers, retaining PCE and inhibiting its downward migration. A multiphase numerical simulator was used to model this sand box experiment. The simulator incorporates wettability-modified van Genuchten and Brooks-Corey capillary pressure/saturation relationships as well as Burdine and Mualem relative permeability relationships. PCE mass distributions, estimated by image analysis of digital photographs taken during the infiltration event, were compared to simulation results. Although both relative permeability models were qualitatively able to predict the PCE retention in the organic-wet layers, simulations with the Mualem model failed to capture the observed rate of PCE migration. A traditional multiphase simulator, incorporating water-wet capillary retention relations, failed to predict both PCE pathways and retention behavior. This study illustrates the potential influence of subsurface wettability variations on DNAPL migration and entrapment and supports the use of modified capillary relations in conjunction with the Burdine model in multiphase flow simulators.

© 2004 Published by Elsevier B.V.

*Keywords:* Multiphase flow; NAPL; Wettability; Heterogeneity; Numerical model; Tetrachloroethylene

\* Corresponding author. Fax: +1-617-627-3819.

*E-mail addresses:* [denismo@engin.umich.edu](mailto:denismo@engin.umich.edu) (D.M. O'Carroll), [sbradford@ussl.ars.usda.gov](mailto:sbradford@ussl.ars.usda.gov) (S.A. Bradford), [Linda.Aabriola@tufts.edu](mailto:Linda.Aabriola@tufts.edu) (L.M. Abriola).

<sup>1</sup> Fax: +1-734-763-2275.

<sup>2</sup> Fax: +1-909-342-4963.

## 1. Introduction

Significant research has focused on the processes governing chlorinated solvent [dense nonaqueous phase liquid (DNAPL)] migration and entrapment following release to the subsurface environment (Kueper et al., 1993; Pennell et al., 1994; Dawson and Roberts, 1997; Hofstee et al., 1998a,b; Bradford et al., 1999; Oostrom et al., 1999a,b). A number of these studies have investigated the effects of subsurface heterogeneity on the fate of DNAPLs. Few, however, have specifically addressed the effects of variations in subsurface wettability.

Wettability refers to the “tendency of one fluid to spread on or adhere to a solid surface in the presence of another immiscible fluid” (Craig, 1971). The contact angle, a measure of wettability, is the angle between the fluid–fluid interface and the solid phase (Hiemenz and Rajagopalan, 1997). In a two-fluid NAPL/water system as the contact angle, measured through the water phase, approaches  $0^\circ$ , the surface is said to be strongly water wetting. Conversely, as the contact angle approaches  $180^\circ$ , the surface is said to be strongly NAPL wetting. Natural materials have a variety of wetting characteristics. For example coal, graphite and talc are intermediate to organic wetting, whereas more common aquifer materials such as quartz and carbonate are water wetting (Anderson, 1987). The condition of mixed wettability, in which the larger pores are oil wetting and the smaller pores are water wetting, has long been recognized in the petroleum industry (Brown and Fatt, 1956; Denekas et al., 1959; Donaldson et al., 1969; Treiber et al., 1972). In addition, wettability can also vary temporally. Researchers have demonstrated that surface active agents in a waste mixture can sorb to mineral surfaces and significantly alter the wettability (Powers and Tamblin, 1995; Lord et al., 2000). The above studies suggest that variations in wettability may be common in the contaminated subsurface. Such variations may influence NAPL migration and persistence in natural settings.

Gravitational, viscous and capillary forces govern the migration and entrapment of NAPLs in the subsurface (Pennell et al., 1996). Capillary forces are a function of the soil texture, the effective contact angle of the porous medium as well as the interfacial properties of the fluids. Thus, variations in medium texture and wettability can significantly affect capillary pressure relations. A number of previous studies have demonstrated the effect of textural variations on NAPL migration in water-wet sandy media, where fine grained materials acted as capillary barriers (Schwille, 1988; Kueper et al., 1989; Illangasekare et al., 1995; Hofstee et al., 1998a,b; Oostrom et al., 1999a,b; Taylor et al., 2001). To date however, the potential influence of variable contact angle on DNAPL migration has not been extensively investigated. Simulated field scale DNAPL infiltration studies suggest that spatial variability in wetting properties can lead to pronounced capillary barriers (Bradford et al., 1998; Phelan et al., in press).

The goal of this study was to explore the effect of spatial variations in wettability on DNAPL migration and entrapment in a controlled sandbox experiment. Experimental observations were then used to assess the predictive capability of a numerical simulator (M-VALOR; Abriola et al., 1992). This simulator had been previously modified to incorporate the influence of wettability on capillary pressure and relative permeability functions to investigate the effects of field scale wettability variations on DNAPL

migration (Bradford et al., 1998). Previous studies utilized the van Genuchten/Burdine or the Brooks Corey/Burdine constitutive relationship and assumed that variations in wettability were correlated with the intrinsic permeability (Bradford et al., 1998; Phelan et al., in press). In this study the appropriateness of a variety of constitutive relationships is assessed and variations in wettability are not correlated to intrinsic permeability.

## 2. Materials and methods

Two types of experiments were undertaken in this work: one-dimensional column studies and a two-dimensional sandbox DNAPL infiltration experiment. The one-dimensional column experiments yielded independent estimates of the conductivity and capillary retention properties of the soils used in the two-dimensional sandbox.

### 2.1. Materials

Laboratory grade (99%) tetrachloroethylene, PCE (Aldrich Chemical, Milwaukee, WI) was selected as the representative DNAPL. The PCE used in the two-dimensional infiltration experiment was dyed with 0.25 g/l of Oil Red O to aid PCE visualization. The aqueous phase was Milli-Q water.

The porous media consisted of various size fractions of Ottawa sand (US Silica, Ottawa, IL), mixed to obtain coarse, medium and fine textural classes. The following 50:50 weight mixtures were used: F20/F30, F35/F50 and F70/F110. The mean grain size and uniformity index for each mixture are provided in Table 1. Organic-wet sands were created by treating the 50:50 sand mixtures with a 5% (by volume) octadecyltrichlorosilane (OTS) in ethanol solution (Anderson et al., 1991). Advancing and receding contact angles for water (in the presence of PCE) were measured on OTS treated quartz slides to be 169° and 148°, respectively (Bradford et al., 1999). These values are consistent with a strongly organic wet system.

### 2.2. One-dimensional columns

Two-phase (water-PCE) capillary pressure/saturation relationships were measured using a pressure cell system based upon the design of Salehzadeh and Demond (1999). Each of the sand mixtures was dry packed in custom designed columns measuring 5 cm ID by 4.8 cm long. Sands were added to the column in 1-cm lifts, compacting each with a wooden plunger and vibrating. Prior to the addition of each lift, the sand surface was roughened to avoid layering. Once packed, the columns were flushed with several pore volumes of carbon dioxide to displace air in the pore space. To saturate the column and completely displace and solubilize the carbon dioxide, the columns were then flushed with 200 pore volumes of Milli-Q water.

Following packing, water-wet and organic-wet ceramic plates (1 or 0.5 bar, Soil Moisture Equipment, Santa Barbara, CA) were attached to the top and bottom of a column, respectively. The bottom of the column was connected to a burette containing PCE and the top was connected to a burette containing water. Each ceramic plate acted as a capillary

Table 1  
Hydraulic Properties for Soils (standard error in parantheses)

	F20/F30 water-wet	F20/F30 organic-wet	F35/F50 water-wet	F35/F50 organic-wet	F70/F110 water-wet
Residual water saturation	0.154	0.100	0.040	0.100	0.245
Residual organic saturation	0.105	0.065	0.200	0.030	0.143 <sup>a</sup>
$\alpha$ – Water drainage – VG (cm H <sub>2</sub> O) <sup>-1</sup>	$1.36 \times 10^{-1}$ ( $1.24 \times 10^{-2}$ )	$1.36 \times 10^{-1}$ ( $1.24 \times 10^{-2}$ )	$5.90 \times 10^{-2}$ ( $3.16 \times 10^{-3}$ )	$5.90 \times 10^{-2}$ ( $3.16 \times 10^{-3}$ )	$2.20 \times 10^{-2}$ ( $3.81 \times 10^{-4}$ )
VG $n$	6.19 (0.60)	6.19 (0.60)	5.63 (0.35)	5.63 (0.35)	9.98 (0.43)
$\eta$ – Water drainage – VG (cm H <sub>2</sub> O)	0.0 (N/A)	8.92 (0.82)	0.0 (N/A)	20.79 (1.42)	0.0 (N/A)
Entry pressure – Water drainage – BC (cm H <sub>2</sub> O)	5.32 (1.36)	5.32 (1.36)	13.77 (1.23)	13.77 (1.23)	37.74 (1.61)
BC $\lambda$	2.95 (0.45)	2.95 (0.45)	3.44 (0.35)	3.44 (0.35)	5.94 (0.64)
$\eta$ – Water drainage – BC (cm H <sub>2</sub> O)	0.0 (N/A)	8.03 (2.17)	0.0 (N/A)	20.42 (2.17)	0.0 (N/A)
Median grain size <sup>a</sup> , $d_{50}$ , cm	0.071	0.071	0.036	0.036	0.015
Uniformity index <sup>a</sup> , $U_i$	1.21	1.21	1.88	1.88	2.25
Permeability (m <sup>2</sup> )	$4.03 \times 10^{-10}$ ( $2.87 \times 10^{-11}$ )	$4.03 \times 10^{-10b}$ ( $2.87 \times 10^{-11b}$ )	$6.38 \times 10^{-11}$ ( $3.07 \times 10^{-12}$ )	$6.38 \times 10^{-11b}$ ( $3.07 \times 10^{-12b}$ )	$4.69 \times 10^{-12}$ ( $1.15 \times 10^{-13}$ )

VG = van Genuchten and BC = Brooks/Corey.

<sup>a</sup> Bradford et al., 1999.

<sup>b</sup> Assumed.

barrier to one of the fluids. This design ensured that the volume of each fluid in the column could be easily determined, given the initial fluid volumes in the burettes and using a simple mass balance calculation. The tops of the burettes were connected to an air pressure/vacuum source, to control the boundary fluid pressures. Fluid flow was induced by imposing a fixed air pressure above the fluid phase in one of the burettes. Fluid volumes in the burettes were estimated using pressure transducer measurements (Micro-Switch, Freeport, IL). Following each incremental increase in fluid pressure, the fluids in the column were equilibrated for 2 h and then the presence of equilibrium was assessed. Equilibrium was assumed achieved when the fluid volumes in the burettes did not change over a 2-h period. Once the system had reached equilibrium the fluid pressure was again incrementally increased. The system described above was fully automated using stepping motors, solenoid valves and a data logger as per Bradford and Leij (1995).

Water wet sand permeabilities were determined using the constant head method proposed by Klute and Dirksen (1986) and are presented in Table 1. The intrinsic permeability was assumed to be unaffected by wettability alterations.

### 2.3. Two dimensional sandbox

PCE infiltration experiments were conducted in a “two-dimensional” sandbox (1.7 cm deep by 30.6 cm wide by 38.4 cm high). The box was constructed with aluminum back and side walls and a tempered glass front, facilitating visual observation of PCE migration. The bottom of the tank was sealed with chemically inert PLV 2100 Base Material Fluoroelastomer viton coating (Pelseal Technologies, Newtown, PA, 18940). Wells at

either end of the box were screened with stainless steel mesh (0.015 cm by 0.015 cm). The volume in each well was approximately  $10 \text{ cm}^3$ .

The system was wet packed in 1–2 cm intervals. Each layer was mixed gently, to minimize layering, packed down with a wooden plunger, and vibrated. Three sand layers were emplaced at the bottom of the tank as shown in Fig. 1. The presence of the lowest 0.6 cm fine water-wet layer (F70/F110) ensured that PCE would not reach the lower aluminum surface. Moving upwards, the sandbox contained a 1.5-cm layer of F20/F30 water-wet sand, followed by a 2.1-cm layer of F20/F30 organic-wet sand. The remainder of the tank was packed with F20/F30 water-wet sand, in which three lenses were emplaced. Two F35/F50 lenses, one organic-wet and the other water-wet, were located 6.2 cm above the aluminum bottom (Fig. 1). The third lens was composed of F70/F110 water-wet sand and was located 17.8 cm above the aluminum base. The entire packed region of the tank had an average porosity of 32.27%. Porosity was estimated by measuring the sand bulk density and assuming a quartz density of  $2.65 \text{ g/cm}^3$  (Danielson and Sutherland, 1986). The effective intrinsic permeability of the packed region ( $3.34 \times 10^{-10} \text{ m}^2$ ) was determined by maintaining constant head boundaries in the inlet and outlet wells and measuring the flow rate at steady state.

A known volume of PCE (47.33 ml) was injected with a syringe pump (Harvard Apparatus, South Natick, MA, 01760) during a 66.6-min period at a constant rate (0.71 ml/min). The injection location was at the midpoint between the glass and the aluminum

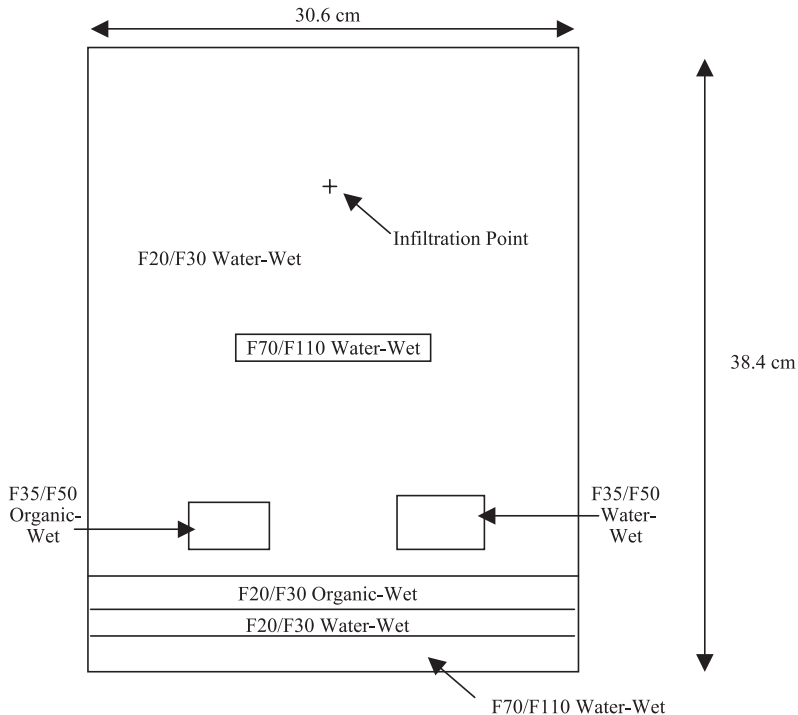


Fig. 1. Schematic representation of two-dimensional sandbox packing (not to scale).

backing, 28.7 cm above the aluminum base (Fig. 1). There was no water flowing during the infiltration experiment, other than that induced by the PCE injection.

The migration of PCE was visually observed and recorded using a digital camera. It should be noted that these observations reflected only the PCE present in the first few millimeters of sand immediately adjacent to the glass. It is assumed here that observed behavior was representative of the entire tank thickness (1.7 cm). Fluid saturations were estimated by correlating the hue of light reflected from the dyed PCE in the system to organic phase saturation (Darnault et al., 1998, 2001). Separate experiments were conducted in small glass cells ( $3.53 \times 3.53 \times 4$  cm) to determine the hue range characteristic of the dyed PCE and the water saturated F20/F30 water-wet sand. PCE was mixed into glass cells containing water saturated F20/F30 water-wet sand to yield a range of PCE saturations. For PCE dyed with 0.25 g/l Oil Red O it was found that the organic phase hue ranged from 0 to 51 in this porous media system. Results from the glass cell experiments yielded a linear relationship ( $R^2=0.91$ ) between the average hue in a glass cell and PCE saturation.

PCE saturations in the larger sandbox were estimated using an organic phase hue range (0–51) based on the small glass cell experiments. Due to variable lighting and differences in glass thickness in the small cells and the larger sandbox, the sum of PCE hue in the larger sandbox was normalized to the total PCE volume in the system. Thus, at a given time, the organic phase hue in each pixel was scaled by the ratio of the sum of the organic phase hue over all pixels and the known volume of PCE in the system to determine PCE saturation. An independent confirmation of this estimation approach is provided by the linear trend between the sum of the organic phase hue over all the pixels and the known total volume of PCE in the system ( $R^2=0.94$ ).

### 2.3. Constitutive relations and numerical model

Capillary pressure/saturation water drainage curves were fit to column data for the five sands used in the two dimensional infiltration experiment. Here both van Genuchten (1980) and Brooks and Corey (1964) capillary pressure/saturation models were modified to incorporate negative capillary pressures. The modified van Genuchten capillary pressure/saturation model is represented as (Bradford and Leij, 1996):

$$P_c = P_o - P_w = \frac{1}{\alpha} (S_w^{\text{app}-1/m} - 1)^{1/n} - \eta \quad (1)$$

where  $P_c$  is the capillary pressure,  $P_o$  is the organic phase pressure,  $P_w$  is the water phase pressure,  $\alpha$  is an empirical constant related to the reciprocal of the entry pressure,  $S_w^{\text{app}}$  is the apparent water saturation,  $n$  is a fitting parameter related to the slope of the capillary pressure/saturation curve,  $m = 1 - 1/n$ , and  $\eta$  is a shifting parameter to account for negative capillary pressures. Similarly, the modified Brooks-Corey capillary pressure/saturation model is expressed as:

$$P_c = P_o - P_w = \frac{1}{\alpha} (S_w^{\text{app}})^{-1/\lambda} - \eta \quad (2)$$

where  $\lambda$  is the pore size index.

For the water/NAPL system the apparent water and NAPL saturations are represented as (Bradford et al., 1998):

$$\begin{aligned}
 S_{\alpha}^{\text{eff}} &= \frac{S_{\alpha} - S_{\alpha i}}{1 - S_{\alpha i} - S_{\beta i}} \\
 S_{\alpha t}^{\text{eff}} &= \frac{S_{\alpha t}}{1 - S_{\alpha i} - S_{\beta i}} \\
 S_{\alpha}^{\text{app}} &= S_{\alpha}^{\text{eff}} + S_{\beta t}^{\text{eff}} - S_{\alpha t}^{\text{eff}} \\
 \alpha &= w, o \quad \beta = o, w
 \end{aligned} \tag{3}$$

where  $S_{\alpha}$  is the actual  $\alpha$ -phase saturation,  $S_{\alpha i}$  is the immobile  $\alpha$ -phase saturation and  $S_{\alpha t}$  is the saturation of the entrapped  $\alpha$ -phase.  $S_{\alpha}^{\text{eff}}$  and  $S_{\alpha t}^{\text{eff}}$  are the effective  $\alpha$ -phase and entrapped  $\alpha$ -phase saturations, respectively.

A nonlinear least squares minimization procedure (SAS 8.01-nlin) was used to fit  $n$  (Eq. (1)),  $\lambda$  (Eq. (2)),  $\alpha$  and  $\eta$  to the experimental data. The immobile water and PCE saturations,  $S_{rw}$  and  $S_{ro}$ , were estimated as the points at which the capillary pressure/saturation curves become vertical for each of the five sands. In this fitting process, it was assumed that  $n$  (Eq. (1)),  $\lambda$  (Eq. (2)) and  $\alpha$  are a function of the particle size distribution and not the wetting characteristics of the sand. Thus, a single set of parameters ( $n$  and  $\alpha$  for Eq. (1);  $\lambda$  and  $\alpha$  for Eq. (2)) was fit to sands having the same particle size distribution, irrespective of their wetting properties. The shifting parameter,  $\eta$ , was fit independently for each of the five sands.

To simulate PCE infiltration in the sandbox, the two-dimensional finite difference multiphase flow simulator M-VALOR (Abriola et al., 1992) was modified to account for variations in wettability by incorporating Eqs. (1) and (2). In addition modified Burdine relative permeability/saturation relationships, based on Burdine (1953), were implemented in the simulator for water-wet and organic-wet soils as (Bradford et al., 1998):

$$k_{rw}^{\text{WaterWet}} = (S_w^{\text{eff}})^2 \frac{\int_0^{S_w^{\text{eff}}} R(S)^2 dS}{\int_0^1 R(S)^2 dS} \quad k_{ro}^{\text{WaterWet}} = (1 - S_w^{\text{eff}})^2 \frac{\int_0^{S_w^{\text{eff}}} R(S)^2 dS}{\int_0^1 R(S)^2 dS} \tag{4a}$$

$$k_{rw}^{\text{OrganicWet}} = (S_w^{\text{eff}})^2 \frac{\int_{1-S_w^{\text{eff}}}^1 R(S)^2 dS}{\int_0^1 R(S)^2 dS} \quad k_{ro}^{\text{OrganicWet}} = (1 - S_w^{\text{eff}})^2 \frac{\int_0^{1-S_w^{\text{eff}}} R(S)^2 dS}{\int_0^1 R(S)^2 dS} \tag{4b}$$

where  $k_{rw}$  and  $k_{ro}$  are the relative permeabilities for water and NAPL, respectively.  $R(S)$  is the pore size distribution that was determined from water-wet capillary pressure/saturation data and LaPlace's equation of capillarity. In the derivation of Eq. (4a) it is assumed that in

water-wet soils water occupies the smaller pores and NAPL occupies the larger pores (Bradford et al., 1999). Conversely in a NAPL-wet soil (Eq. (4b)) it is assumed that NAPL occupies the smaller pores and water occupies the larger pores.

Using these same assumptions the Mualem (1976) relative permeability model was also modified for application to both water-wet and organic-wet soils as:

$$k_{rw}^{\text{WaterWet}} = (S_w^{\text{eff}}) = (S_w^{\text{eff}})^{0.5} \left[ \frac{\int_0^{S_w^{\text{eff}}} R(S) dS}{\int_0^1 R(S) dS} \right]^2 \quad (5a)$$

$$k_{ro}^{\text{WaterWet}}(S_w^{\text{eff}}) = (1 - S_w^{\text{eff}})^{0.5} \left[ \frac{\int_{S_w^{\text{eff}}}^1 R(S) dS}{\int_1^0 R(S) dS} \right]^2$$

$$k_{rw}^{\text{OrganicWet}}(S_w^{\text{eff}}) = (S_w^{\text{eff}})^{0.5} \left[ \frac{\int_{1-S_w^{\text{eff}}}^1 R(S) dS}{\int_0^1 R(S) dS} \right]^2 \quad (5b)$$

$$k_{ro}^{\text{OrganicWet}}(S_w^{\text{eff}}) = (1 - S_w^{\text{eff}})^{0.5} \left[ \frac{\int_0^{1-S_w^{\text{eff}}} R(S) dS}{\int_0^1 R(S) dS} \right]^2$$

Eqs. (4a), (4b), (5a) and (5b) were incorporated into the M-VALOR simulator. This simulator also incorporates non-wetting fluid entrapment and the corresponding reduction in available pore space, using an algorithm based on Lenhard and Parker (1987).

The infiltration experiment was modeled using the modified M-VALOR simulator. The modeled domain was discretized uniformly, with 33 nodes in the horizontal (1.0 cm spacing) and 70 nodes in the vertical (0.5 cm spacing). This grid resolution was selected based on a sensitivity study conducted by Rathfelder et al. (2003). The bottom of the tank was considered a no flow boundary and the top and side boundaries were modeled as constant head boundaries, based upon observed water elevations in the wells. Although PCE was free to migrate into the wells, at either side of the tank, this condition was not observed. For the simulations it was assumed that the capillary properties of the stainless steel mesh screening the wells were the same as the water-wet 20/30 sand; in addition the steel mesh porosity was assumed as 0.75 and the permeability  $4.08 \times 10^{-9} \text{ m}^2$ , an order of magnitude greater than the F20/F30 sand.



### 3. Experimental results and discussion

#### 3.1. One-dimensional columns

Representative comparisons of fitted and observed primary water drainage capillary pressure saturation relations (for the F20/F30 water and organic-wet Ottawa sands) are presented in Fig. 2. Fitted and observed capillary pressure curves for the F35/F50 and F70/F110 sands exhibited similar behavior and are not presented. Note that the modified van Genuchten and Brooks-Corey fits are similar except at high water saturations. Fitted capillary parameters for all sands are presented in Table 1 along with their standard error. Entry pressures for the three sands follow expected trends. An increase in the median grain size results in a decrease in sand entry pressure (Table 1).

In contrast to its behavior in the water-wet sands, PCE spontaneously imbibes into organic-wet sands. Fig. 2 reveals that, in the organic wet F20/F30 sand, the water saturation must decrease below approximately 40% before a positive capillary pressure is required to displace the water during primary water drainage. A similar behavior was observed for the organic-wet F35/50 sand.

Predicted Brooks-Corey/Burdine and Brooks-Corey/Mualem relative permeability relationships for both water-wet and organic-wet F20/F30 sands are presented in Fig. 3. Here Eq. (2) is used along with fitting parameters from Table 1 in Eqs. (4a)–(5b), respectively, to produce the plotted curves. Trends in relative permeability predictions for the F35/F50 and F70/F110 sands are similar. Notice that, at a given saturation, the Mualem relative permeability is larger than that obtained using the Burdine equation. In addition, when a fluid is non-wetting, its predicted relative permeability is larger, at a given

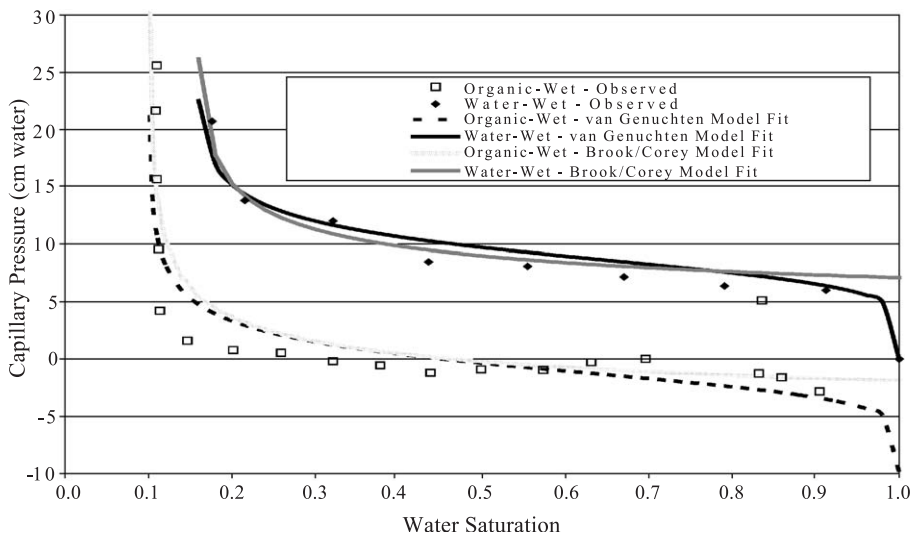


Fig. 2. Observed and fit primary water drainage capillary pressure relationship for water-wet and organic-wet F20/F30 Ottawa sand.

saturation, than it would be if it were the wetting fluid, i.e. water relative permeability is larger in the organic-wet sand than in the water-wet sand. This prediction is a consequence of the assumption that the non-wetting fluid occupies the larger pores. The van Genuchten/Burdine and van Genuchten/Mualem relative permeability models for these sands exhibited similar trends (not shown).

### 3.2. Two dimensional sandbox PCE infiltration

Figs. 4c, 5c, 6c and 7c present photos of the PCE infiltration experiment at specific times following the initiation of the PCE injection. Upon release, the PCE migrated down to the F70/F110 sand lens and pooled on top. Further downward migration did not occur until the PCE pooled and migrated laterally cascading over the sides of the lens. Here the PCE did not reach a pressure head sufficient to penetrate the F70/F110 lens (52.74 cm H<sub>2</sub>O, assuming static water conditions).

Similar pooling and cascading behavior occurred when the PCE reached the water-wet F35/F50 lens. Here again, the PCE head did not exceed that required (39.77 cm H<sub>2</sub>O, assuming static water conditions) to penetrate the water-wet F35/F50 lens. Above this lens, PCE migration was not strictly vertical as originally anticipated; a portion of the PCE bypassed the water-wet F35/F50 lens on the right side of the tank. This volume migrated directly down to the organic-wet F20/F30 layer, where it was retained. This PCE bypassing may be attributed to the presence of small-scale heterogeneities (Kueper et al., 1993). Although no large-scale packing heterogeneities existed in the sandbox it was

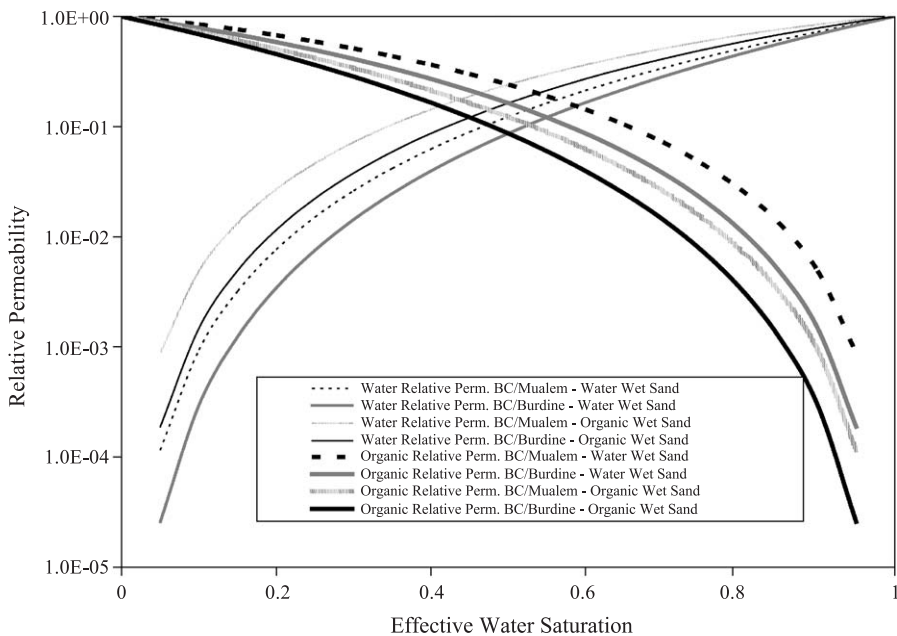


Fig. 3. Predicted relative permeability relationship for F20/F30 Ottawa sand.

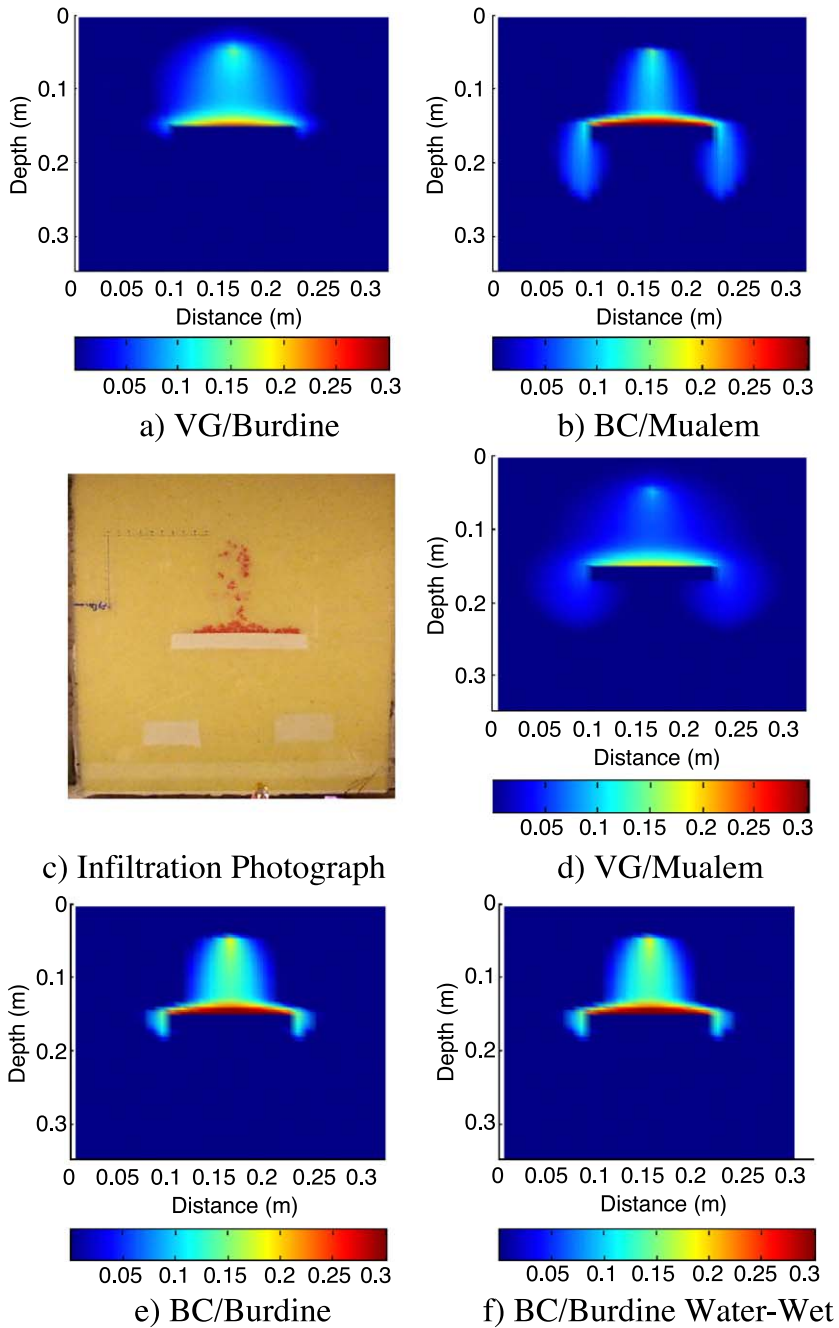


Fig. 4. Two-dimensional infiltration photo and simulations at elapsed time = 10 min.

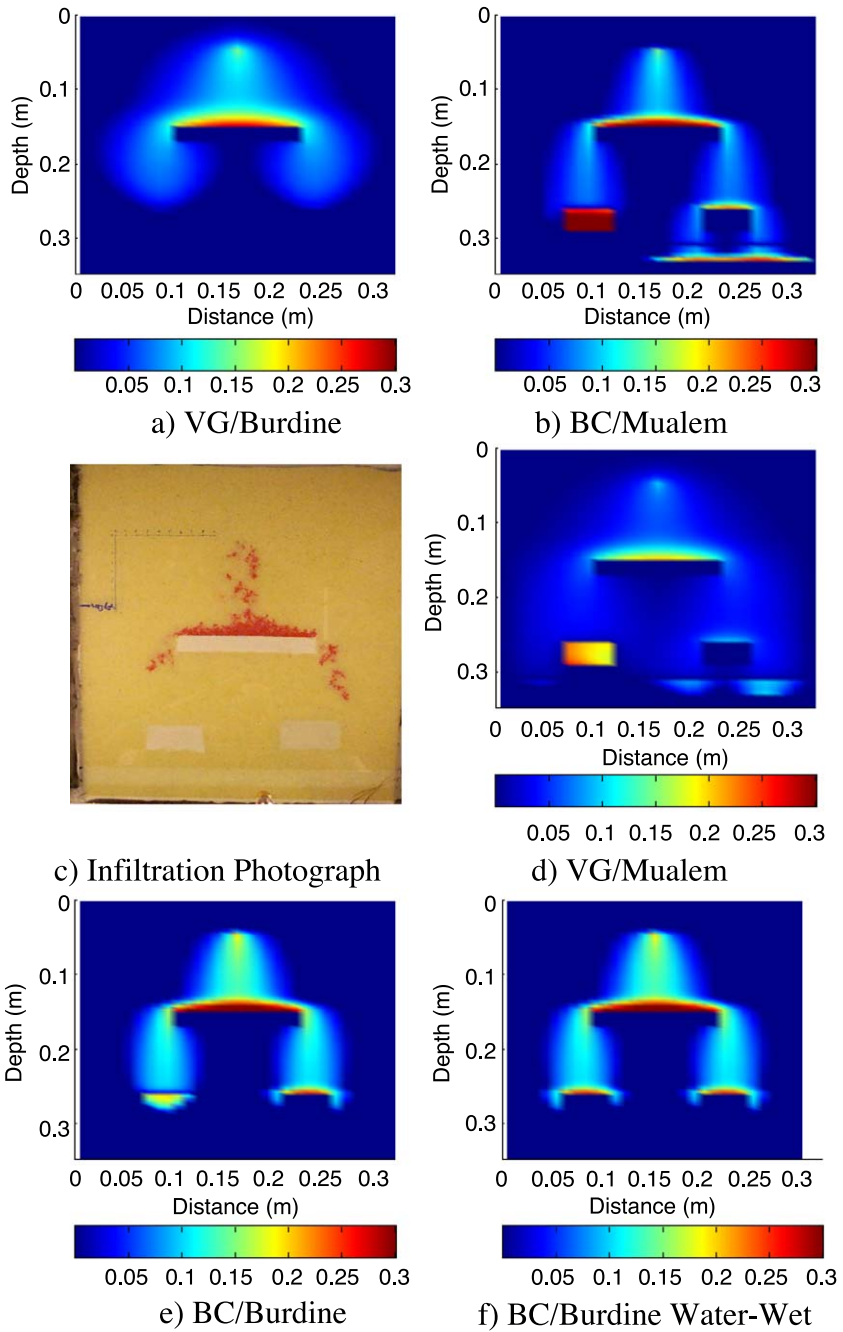


Fig. 5. Two-dimensional infiltration photo and simulations at elapsed time=20 min.

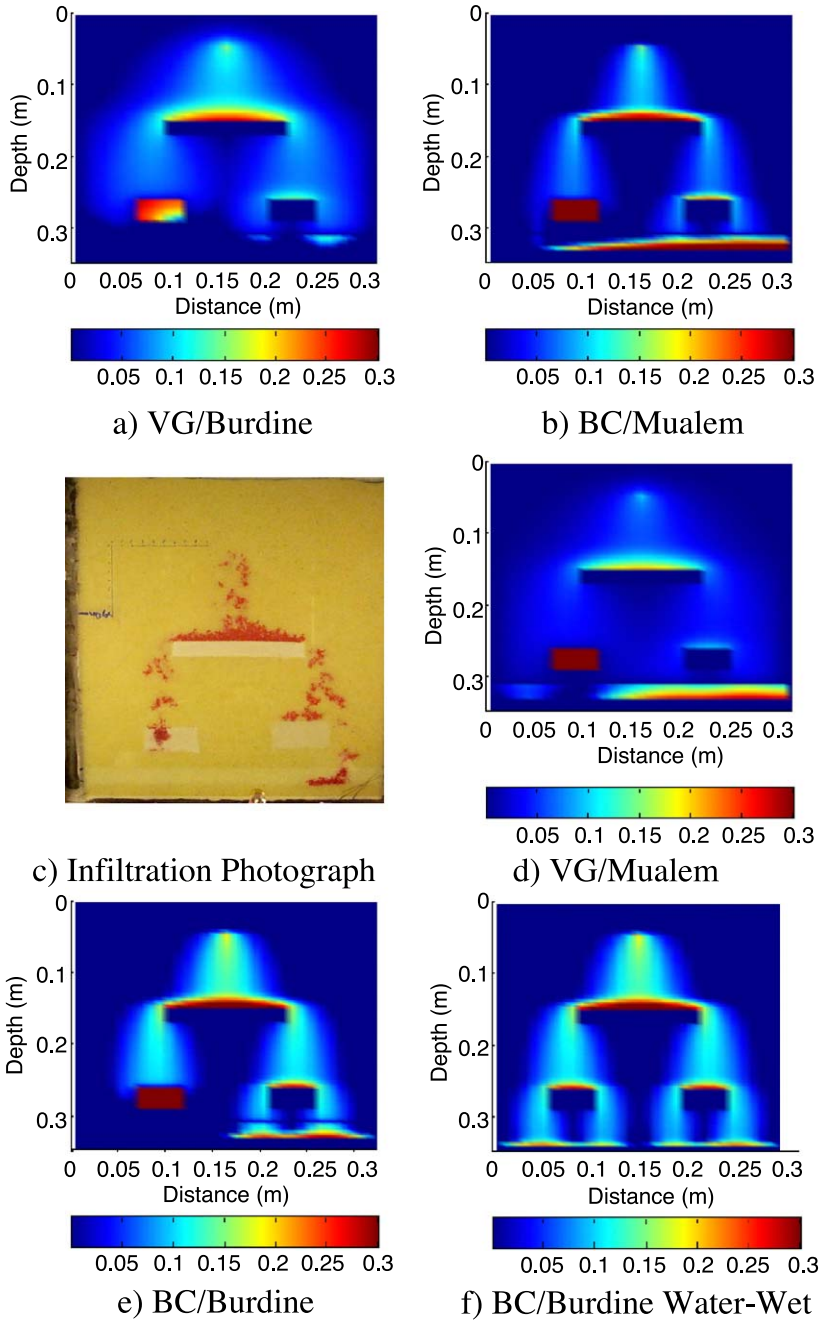


Fig. 6. Two-dimensional infiltration photo and simulations at elapsed time = 30 min.

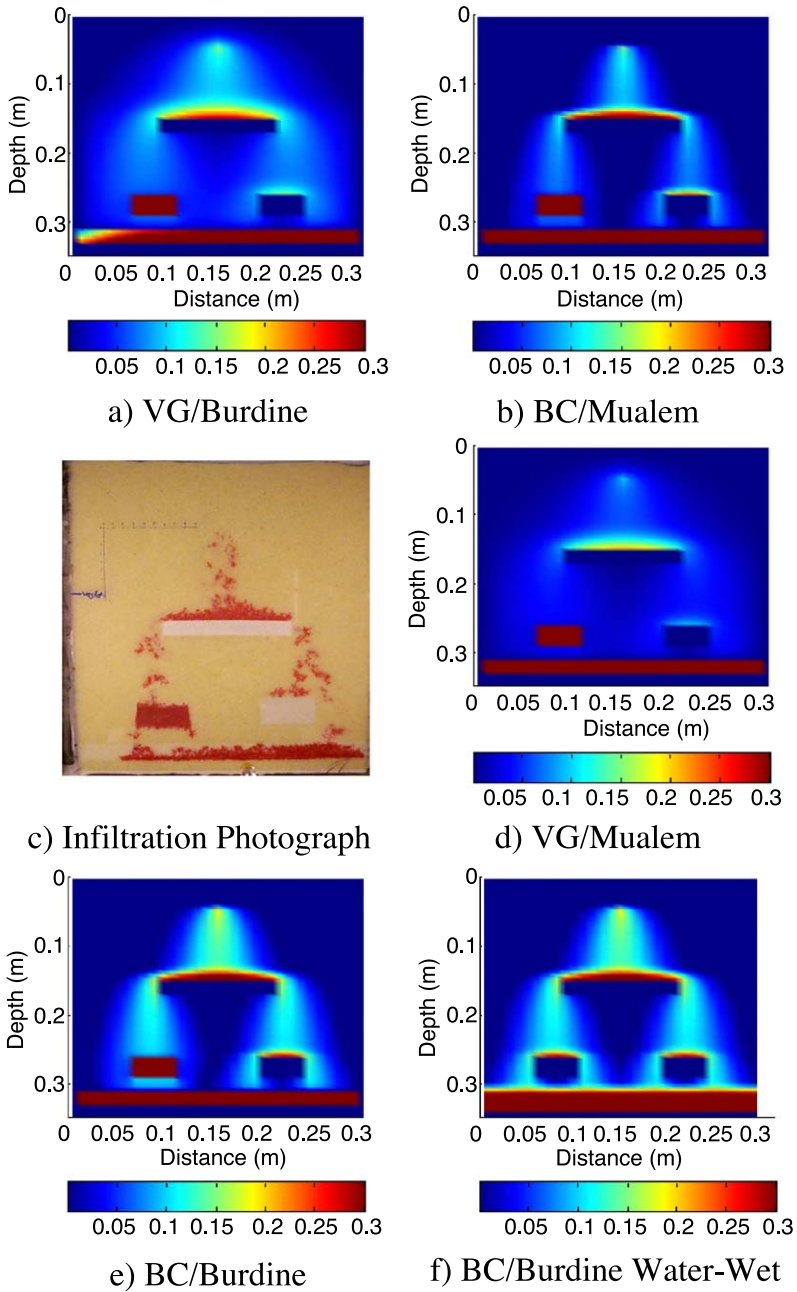


Fig. 7. Two-dimensional infiltration photo and simulations at elapsed time=60 min.

impossible to completely eliminate small-scale variations in porosity. As a result the PCE may have followed non-vertical pore scale pathways of higher hydraulic conductivity within the F20/F30 sand, permitting it to bypass the F35/F50 lens. Other researchers have measured variations in bulk density in similar sandbox infiltration experiments and attributed observed PCE fingering to these variations (Rathfelder et al., 2003).

In contrast, on the left side of the tank, the PCE spontaneously imbibed into the organic-wet F35/F50 lens. The negative capillary entry pressure for the F35/F50 organic-wet lens facilitated PCE migration into this lens. Continued downward migration of PCE through this organic-wet lens occurred only after the lens neared complete PCE saturation, as seen in Figs. 6c and 7c.

PCE that migrated beyond the F35/F50 lenses was retained by the F20/F30 organic-wet layer near the bottom of the tank. No PCE migrated into the water-wet F20/F30 layer below the organic-wet layer. These visual observations of PCE infiltration indicate that organic-wet sands can act as a very effective capillary barrier, retaining PCE and inhibiting its downward migration. After 60 min of PCE infiltration, high PCE saturations were present in the organic-wet F20/F30 and F35/F50 lenses, whereas low PCE saturations were present in the exposed F20/F30 water-wet sands. No PCE migrated into the wells at either side of the tank.

### 3.3. Simulation results

Results of five simulations are presented in Figs. 4–7 for comparison with the infiltration experiment photos. Simulations incorporating the van Genuchten/Burdine (a), Brooks-Corey/Mualem (b), van Genuchten/Mualem (d) and Brooks-Corey/Burdine (e) capillary pressure/relative permeability/saturation models are presented. Each of these simulations takes into account the variable wettability in the sand tank. Experimental observations are compared quantitatively with simulations in Tables 2, 3 and 4. The location of the center of PCE mass, based on image analysis and simulation results, is presented in Table 2. The second PCE mass moments about the horizontal and vertical axes (vertical and horizontal PCE spread; Phelan et al., in press) are presented in Tables 3 and 4. A completely water-wet prediction, using the Brooks-Corey/Burdine (f) model, is also shown.

In Figs. 4–7 plotted simulation saturation contours range from 1% to 30%. The lower PCE saturation limit of 1% was selected to correspond with the results of the image analysis and allows easy comparison between simulation results and experimental observations. The upper saturation limit of 30% facilitates optimal visualization of PCE migration pathways in the water-wet sand. Estimated and predicted saturations in the water-wet F20/F30 sand are below 30% in areas other than the localized area immediately above the F70/F110 lens.

The location of the PCE center of mass, based on image analysis of the experimental results, is similar to that of the van Genuchten/Burdine, van Genuchten/Mualem and Brooks-Corey/Burdine simulations at 10 min (Fig. 4a, d and e, respectively, and Table 2). The simulations that utilize the Burdine model predict that the majority of the PCE is flowing down to and pooling on top of the F70/F110 lens, with only a small fraction cascading over the edge of the lens. Experimental observations, however, indicate that the PCE has cascaded down to the F70/F110 lens but has not reached its edge. Thus, the

Table 2

Depth of the Center of PCE Mass from the Injection Location (cm)

Time	10 min	20 min	30 min	60 min	RMSE
Image Analysis	8.0	9.0	13.8	19.5	
van Genuchten/Burdine	6.3	9.4	13.1	18.8	0.99
Brooks-Corey/Mualem	11.1	16.2	19.3	23.3	5.17
van Genuchten/Mualem	9.3	14.0	17.5	21.9	3.39
Brooks-Corey/Burdine	7.9	11.8	15.9	21.1	1.93

observed horizontal spread of PCE is significantly less than that predicted by the Burdine model (Table 3). Simulations that utilize the Mualem relative permeability constitutive relationship have a larger horizontal spread at 10 min. In these simulations 35–40% of the injected PCE has flowed laterally around the F70/F110 lens. The increased depth of PCE penetration, and therefore the larger horizontal spread, for the simulations that incorporate the Mualem model is anticipated based upon the larger magnitude of the organic relative permeability predicted using the Mualem model in comparison to the Burdine model.

At 20 min the van Genuchten/Burdine model simulation is consistent with the experimental observations in terms of average depth of PCE penetration. Visual observations reveal that PCE has cascaded over the sides of the water-wet F70/F110 lens but has not yet reached either of the F35/F50 lenses (Fig. 5c and a, respectively). In contrast, the Brooks-Corey/Mualem and van Genuchten/Mualem simulations predict that PCE has reached the organic-wet F20/F30 lens near the bottom of the tank (Fig. 5b and d). As a result, the predicted location of center of PCE mass for these simulations is considerably deeper than experimental observations. A consequence of the depth of the center PCE mass is the significant vertical spread of PCE for these simulations (Table 4). Although the Brooks-Corey/Burdine simulation predicts that PCE reaches the F35/F50 lenses in 20 min, it has only begun to enter the organic-wet F35/F50 lens and to accumulate on top of the water-wet F35/F50 lens. Thus, the van Genuchten/Burdine and Brooks-Corey/Burdine simulations bracket observed behavior; the observed configuration of PCE migration is similar to that obtained with the Brooks-Corey/Burdine simulation and the migration rate is similar to that predicted in the van Genuchten/Burdine simulation. Other researchers have made similar observations pertaining to the Burdine model. Oostrom and Lenhard (1998) and Schroth et al. (1998) compared one- and two-dimensional infiltration experimental observations to simulations using the Brooks-Corey/Burdine and van Genuchten/Mualem constitutive relationships. These researchers concluded that simula-

Table 3

Second PCE mass moment about the vertical axis through the injection point (horizontal spread—m<sup>2</sup>)

Time	10 min	20 min	30 min	60 min
Image analysis	$7.2 \cdot 10^{-4}$	$2.6 \cdot 10^{-3}$	$5.2 \cdot 10^{-3}$	$5.9 \cdot 10^{-3}$
van Genuchten/Burdine	$2.4 \cdot 10^{-3}$	$4.5 \cdot 10^{-3}$	$9.8 \cdot 10^{-3}$	$3.4 \cdot 10^{-2}$
Brooks-Corey/ Mualem	$3.3 \cdot 10^{-3}$	$4.3 \cdot 10^{-3}$	$4.8 \cdot 10^{-3}$	$6.7 \cdot 10^{-3}$
van Genuchten/Mualem	$4.5 \cdot 10^{-3}$	$1.7 \cdot 10^{-2}$	$3.4 \cdot 10^{-2}$	$5.1 \cdot 10^{-2}$
Brooks-Corey/Burdine	$2.2 \cdot 10^{-3}$	$3.8 \cdot 10^{-3}$	$4.5 \cdot 10^{-3}$	$6.1 \cdot 10^{-3}$



tions using the Burdine relative permeability model were better able to predict NAPL migration behavior.

Similar to results at 20 min both Mualem simulations, at 30 min, predict PCE migration that is faster than the experimental observations (Fig. 6b and d, Table 2). On the other hand, the van Genuchten/Burdine and Brooks-Corey/Burdine simulation results compare reasonably well with the experimental observations in terms of penetration of the center of PCE mass (Fig. 6a, e and c, respectively, Table 2). PCE has started to imbibe into the organic-wet F35/F50 sand and pond on top of the water-wet F35/F50 lens. The van Genuchten/Burdine simulation, however, predicts lateral spreading in the F35/F50 organic-water sand that was not observed experimentally (Table 3). Similar capillary spreading behavior is observed for the van Genuchten/Mualem simulation and has been reported by other investigators and attributed to the capillary driving force of the van Genuchten model at high water saturations (Ostrom and Lenhard, 1998; Rathfelder and Abriola, 1998; Schroth et al., 1998; Rathfelder et al., 2000).

Results of the image analysis at 30 min are presented in Fig. 8. Here observed PCE saturations are much higher immediately above the F70/F100 lens in comparison with simulated saturations. In this pool PCE saturations reach 71% whereas the simulations predict maximum PCE saturations of only 38%. In addition to the high PCE saturations above this lens, the extent of this high saturation zone is larger than the simulations suggest. Given the combination of higher PCE saturations and larger pool extent, above this lens, much more PCE is retained in this region than predicted by the simulations.

All simulations predict appreciable PCE saturations along the top of the entire F35/F50 organic-wet lens, allowing PCE to enter the lens across the entire interface. In contrast, experimental observations suggest that PCE only entered the organic-wet lens through a portion of the interface. The simulations, thus, predict more uniform penetration of the organic-wet lens, whereas image analysis indicates that high PCE saturations were localized in a portion of the lens. Experimental observations revealed the PCE began to spread laterally in the organic-wet F35/F50 lens only when it had reached its lower interface with the water-wet F20/F30 sand. Because the sandbox simulations predicted more uniform infiltration into the organic-wet lens, experimental model comparisons did not facilitate evaluation of the ability of the chosen capillary relations to predict the degree of lateral spreading within the organic-wet lens.

To test the predictive capabilities of the organic-wet capillary pressure/saturation models, additional simulations were conducted in which half of the injected PCE (23.67 ml) was released immediately above the organic-wet F35/F50 lens to mimic experimental observations. Here it was assumed that approximately half of the infiltrated PCE reached

Table 4  
Second PCE mass moment about the horizontal axis through the center of PCE Mass (vertical spread— $m^2$ )

Time	10 min	20 min	30 min	60 min
Image analysis	1.1e – 03	1.0e – 03	4.6e – 03	5.6e – 03
van Genuchten/Burdine	1.4e – 03	2.9e – 03	5.4e – 03	7.4e – 03
Brooks-Corey/ Mualem	3.0e – 03	6.0e – 03	6.0e – 03	4.7e – 03
van Genuchten/Mualem	2.8e – 03	6.0e – 03	7.2e – 03	6.2e – 03
Brooks-Corey/Burdine	1.4e – 03	3.6e – 03	5.9e – 03	6.1e – 03

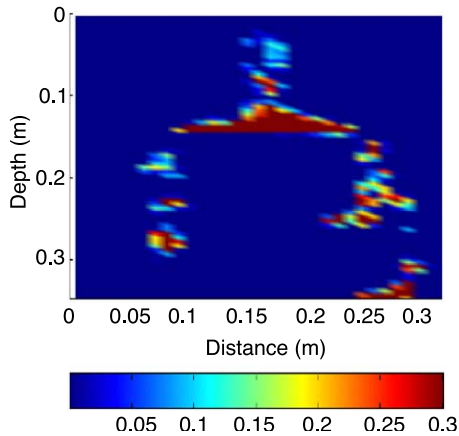


Fig. 8. Estimated organic phase saturations at elapsed time = 30 min.

the organic-wet F35/F50 lens in the experiment. These simulations (not shown) predicted more lateral PCE spread within the organic-wet lens than was observed experimentally. As the PCE entered the simulated organic-wet lens it spread both laterally and downwards through the lens, whereas experimental observations indicated minimal lateral spread following penetration of the lens. Lord (2002) measured two-phase (water-PCE) capillary pressure/saturation relationships for F35/F50 sand with the same organic coating. In contrast to the capillary pressure/saturation experimental results for organic-wet F35/F50 sand presented here, Lord (2002) did not observe negative capillary pressures during primary water drainage. An additional simulation, similar to the ones discussed above, was conducted to test the predictive capabilities of the simulator using parameters fit to these alternative capillary pressure data. Similar to the experimental observations, this simulation predicted that lateral PCE spread in the organic-wet F35/F50 lens occurred only when it reached the lower water-wet F20/F30, organic-wet F35/F50 sand interface. Based on these simulations it is clear that the organic-wet capillary pressure/saturation expressions with negative capillary pressures on the primary water drainage branch do not adequately reproduce the observed migration of PCE within the organic-wet materials in the 2-D infiltration event. Clearly capillary forces did act to retain PCE in the F35/F50 organic-wet lens and inhibit further downward migration into the underlying F20/F30 water-wet sand. The F35/F50 organic-wet curve, therefore, behaved as though it had a substantially lower entry pressure than the water-wet material of the same gradation. Further work is required to investigate the discrepancy in the organic-wet F35/F50 capillary pressure/saturation measurements along the primary water drainage branch.

Another important observation at 30 min is that a portion of the PCE bypassed the water-wet F35/F50 lens, as outlined in the previous section. The homogeneous model cannot capture this behavior. Other researchers have incorporated small scale variations in bulk density in numerical simulations of sandbox infiltration experiments (Rathfelder et al., 2003). Incorporation of these variations permitted model predictions to capture observed fingering behavior in a qualitative sense. Precise prediction of bypassing pathways, as

observed in the present work, however would require perfect knowledge of porosity variations at an extremely fine-scale resolution.

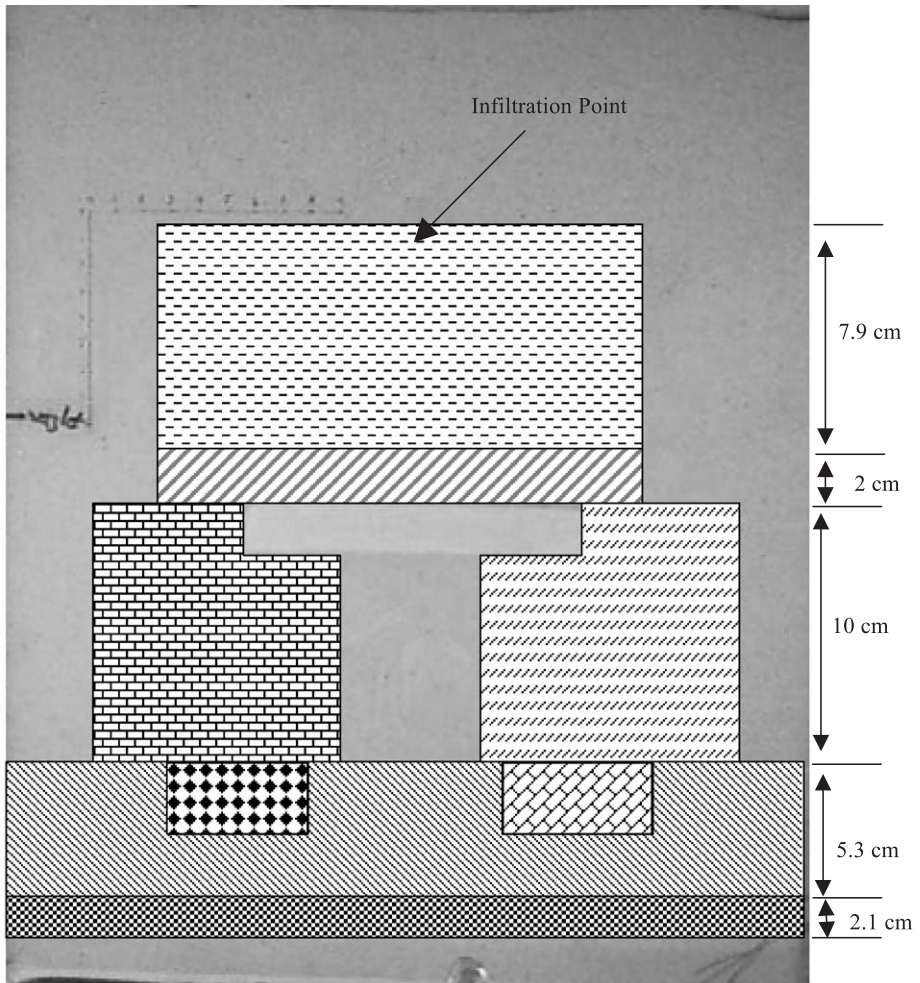
As simulated and experimental time progress PCE continues to imbibe into both the organic-wet F35/F50 lens and the organic-wet F20/F30 layer. Both simulated and experimental results indicate that the majority of the PCE enters the right side of the organic-wet F20/F30 layer and moves from right to left in this layer. This is expected given that the organic-wet F35/F50 lens effectively holds up the PCE front at the left side of the sandbox. Only when the organic-wet F35/F50 lens is nearly saturated with PCE is there continued downward PCE migration. At 60 min, simulations predict that the F35/F50 organic-wet lens is effectively saturated with PCE retaining 15% of the infiltrated volume, consistent with experiment observations (see Table 5 and Fig. 9).

Further comparison of the predicted and observed mass distribution at 60 min suggests that significantly more PCE is retained in Region 2, immediately above the F70/F110 lens (Fig. 9 and Table 5) than predicted by the simulations. These results are similar to those previously discussed for an elapsed time of 30 min. Consistent with the experimental observations, all simulations predict a significant amount of PCE entrapment in the F20/F30 layer near the tank bottom, Region 8 (Fig. 9 and Table 5). Due to its faster predicted rate of propagation and minimal capillary spreading, the Brook-Corey/Mualem simulation predicts the largest PCE mass in the F20/F30 organic-wet layer (Table 5). Conversely, the van Genuchten/Burdine simulation predicts the slowest PCE migration and the lowest PCE entrapment in the F20/F30 organic-wet layer at 60 min. Although the simulations predict that the majority of the PCE enters the right side of the organic-wet F20/F30 layer, they also predict that PCE will enter, at very low saturations, through the entire top interface of the organic-wet F20/F30 layer. Thus, simulations predict that appreciable PCE saturations will be present throughout the organic-wet F20/F30 layer at 60 min. In comparison, experimental observations indicate that high PCE saturations were present only at the right side of the tank (Fig. 7). Given the appreciable simulated spreading, as PCE enters the organic-wet F20/F30 layer, simulated saturation distributions were insensitive to the relative permeability model selected for the organic-wet sands. Thus, it is not possible to distinguish among organic-wet relative permeability models.

To determine which model best predicts the mass distribution of PCE in the system, the root mean square prediction error (RMSE) was calculated. In this calculation, the

Table 5  
Estimated and Simulated PCE % mass distribution at 60 minutes

	Image analysis	van Genuchten/ Burdine	Brooks-Corey/ Burdine	Brooks-Corey/ Mualem	van Genuchten/ Mualem
Region 1	8	14	9	5	8
Region 2	17	7	8	6	5
Region 3	5	9	8	5	5
Region 4	10	10	9	6	5
Region 5	17	15	15	15	15
Region 6	4	6	6	4	3
Region 7	0	0	0	0	0
Region 8	39	27	43	59	43
RMSE		6.1	3.9	8.3	4.9






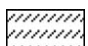




- |   |   |
|---|---|
|  Region 1: 20/30 Water-Wet   |  Region 2: 20/30 Water-Wet   |
|  Region 3: 20/30 Water-Wet   |  Region 4: 20/30 Water-Wet   |
|  Region 5: 35/50 Organic-Wet |  Region 6: 20/30 Water-Wet   |
|  Region 7: 35/50 Water-Wet   |  Region 8: 20/30 Organic-Wet |

Fig. 9. Regions of two-dimensional sandbox exposed to the organic phase.

simulated mass of PCE in a given region (Fig. 9) was subtracted from that estimated from experimental observations. RMSE results indicate that the Brooks-Corey/Burdine model resulted in the best predictions of mass distribution (Table 5). In addition, the second PCE mass moments about the horizontal and vertical axes (horizontal and vertical spread) for the Brooks-Corey/Burdine simulations are generally closest to the experimental observations (Tables 3 and 4). Although the mass distribution is best approximated using the Brooks-Corey/Burdine model, the rate of PCE migration is best approximated by the van Genuchten/Burdine model. This can be seen by examining the RMSE of the depth of the center of PCE mass (Table 2).

Simulations with the van Genuchten capillary pressure/saturation model predict PCE mass would be lost through the wells at either side of the sand box. The van Genuchten/Mualem simulation predicts 11% PCE mass loss, whereas the van Genuchten/Burdine simulation predicts 6% PCE mass loss at 60 min. Simulations that used the Brooks-Corey capillary pressure/saturation model, however, predict no PCE mass loss. No PCE loss was observed during the experiment.

It is important to note that there is some uncertainty associated with the intrinsic permeability measurements and fit capillary retention properties. Simulations were carried out to determine the potential influence of this uncertainty (in terms of the standard error associated with each property) on model predictions (not presented). These simulation results indicate that maximum differences in PCE mass distribution, the location of the center of PCE mass and vertical and horizontal PCE spread were less than 3.5% when each parameter was varied within its standard error. The overall trends in comparisons among simulations employing the four capillary pressure/relative permeability/saturation relationships remained the same.

### 3.4. Comparison of simulation results in a completely water wet system

It is traditionally assumed that porous media in the subsurface are water-wet when modeling DNAPL spill events. In order to assess the error associated with this assumption, a Brooks-Corey/Burdine simulation of the infiltration event was conducted with a completely water-wet model domain of the same physical properties. When constant head side boundary conditions were employed on the sides of the box, the simulator predicted that the majority of the PCE would migrate to the bottom of the tank and then laterally to the wells and out of the system. Thus, the side boundary conditions were changed to no flow and the simulations repeated. These simulation results with the completely water-wet domain are presented in Figs. 4f–7f.

Comparison of the water-wet simulation results with those of the other models indicates that front migration is similar at 10 min (Fig. 7f). This result confirms that no-flow and constant head side boundary conditions yield similar results under these experimental conditions. Simulation results differ at 20 min, when the organic begins to imbibe in the F35/F50 organic-wet lens. The completely water-wet domain simulation predicts that the PCE will simply cascade over the lens and not imbibe into it. At 30 min, the completely water-wet simulation predicts that the plume migrates beyond the F35/F50 lenses and is retained just above the F70/F110 layer at the bottom of the tank. In reality the PCE does not reach the F70/F110 layer because it is retained in the F20/F30 organic-wet layer.

By comparing the completely water-wet simulation to the other simulations it is clear that the water-wet assumption yields drastically different predictions (Figs. 4–7). At 60 min, simulations that take wettability variations into account, predict that approximately 15% of the infiltrated PCE volume was retained in the F35/F50 organic-wet lens and between 30% and 60% of the infiltrated volume was retained in the F20/F30 organic-wet layer. The water-wet simulation does not predict that PCE is retained at either location.

#### **4. Summary and conclusions**

A coupled laboratory/modeling investigation was undertaken to quantify the effect of spatial wettability variations on DNAPL migration and entrapment. Sand column experiments were conducted on coarse, medium and fine textured water-wet and organic-wet sands to determine capillary pressure/saturation relationships. For the tested organic-wet sands, PCE spontaneously imbibed into the columns at high water saturations. Due to the strong dependence of NAPL hydraulic properties on wettability, wettability-modified van Genuchten and Brooks-Corey models were successfully fit to the capillary pressure/saturation data.

A two-dimensional infiltration experiment was conducted to visually observe the effect of spatial wettability variations on DNAPL migration and entrapment. Experimental results indicate that interfaces of capillary property contrast lead to higher NAPL saturations, increased lateral spreading, and decreasing depths of NAPL infiltration. The organic-wet sands effectively retained PCE and inhibited further downward migration.

A multiphase numerical simulator, modified to account for the influence of wettability variations on hydraulic property relations, was then used to simulate the sand box experiment. In the model, measured capillary pressure/saturation relationships were employed and relative permeability relationships were estimated based on pore size distribution and wettability. Simulations results were compared to experimental PCE mass distributions, generated using image analysis. All simulations that accounted for varying wettability accurately predicted the observed PCE migration pathways (i.e. retention of PCE in the organic-wet layers). The two simulations that utilized the Mualem relative permeability model predicted PCE migration at a rate faster than observed experimentally, whereas the two simulations that incorporated the Burdine relative permeability model adequately predicted depth of the center of PCE mass. These results suggest that the Burdine relative permeability/saturation relationship is more appropriate than the Mualem relative permeability/saturation relationship for two-phase liquid flow modeling in the water-wet sands. Observed organic infiltration and spreading behavior within the organic-wet lenses was not well-modeled by the simulations. Further experiments will be needed to explore the appropriate relative permeability model in organic-wet sands, to investigate the degree of capillary spreading and to determine the appropriate primary water drainage capillary pressure/saturation relationship in these materials. It is also important to note that simulations utilizing the van Genuchten capillary pressure/saturation model resulted in prediction of PCE mass loss from the system that was not observed experimentally. A numerical simulation was also carried out with a completely water-wet domain. This

simulation led to large errors in the prediction of the depth of PCE penetration, its degree of retention in the porous medium and its rate of propagation.

These experimental observations and numerical simulations illustrate the potential influence of subsurface wettability variations on DNAPL migration and entrapment. Although the OTS coated materials employed herein were extremely hydrophobic, there is mounting evidence that porous media at many contaminated sites are not completely water-wet. At such sites it is anticipated that a portion of the porous media will act to retain some of the DNAPL, thereby acting as a long-term source of aqueous phase contamination. Knowledge of the aqueous phase chemistry, variations in grain mineralogy, the presence of organic matter, and/or interactions of the formation solids and surface active organic contaminants is therefore required to determine the extent of variable soil wettability. Incorporation of wettability effects in numerical simulators and adequate quantification of subsurface wettability will result in improved predictions of the fate of DNAPLs in the subsurface.

## Acknowledgements

This research was supported in full by Grant No. DE-FG07-96ER14702, Environmental Science Program, Office of Science and Technology, Office of Environmental Management, United States Department of Energy (DOE). Any opinions, findings, conclusions, or recommendations expressed herein are those of the authors and do not necessarily reflect the views of DOE.

## References

- Abriola, L.M., Rathfelder, K.M., Maiza, M., Yadav, S., 1992. Valor code version 1.0: A pc code for simulating immiscible contaminant transport in subsurface systems. EPRI TR-101018, EPRI TR-101018.
- Anderson, W.G., 1987. Wettability literature survey: Part 4. Effects of wettability on capillary pressure. *Journal of Petroleum Technology* 39, 1283–1300.
- Anderson, R., Larson, G., Smith, C., 1991. Silicon compounds: register and review. Huls America, Piscataway, NJ.
- Bradford, S.A., Leij, F.J., 1995. Fractional wettability effects on 2-fluid and 3-fluid capillary pressure–saturation relations. *Journal of Contaminant Hydrology* 20 (1–2), 89–109.
- Bradford, S.A., Leij, F.J., 1996. Predicting two- and three-fluid capillary pressure saturation relationships of porous media with fractional wettability. *Water Resources Research* 32 (2), 251–259.
- Bradford, S.A., Abriola, L.M., Rathfelder, K.M., 1998. Flow and entrapment of dense nonaqueous phase liquids in physically and chemically heterogeneous aquifer formations. *Advances in Water Resources* 22 (2), 117–132.
- Bradford, S.A., Vendlinski, R.A., Abriola, L.M., 1999. The entrapment and long-term dissolution of tetrachloroethylene in fractional wettability porous media. *Water Resources Research* 35 (10), 2955–2964.
- Brooks, R.H., Corey, A.T. (Eds.), 1964. Hydraulic properties of porous media. *Hydrology*, vol. 3. Civil Engineering Department, Colorado State University, Boulder, CO.
- Brown, R.J.S., Fatt, I., 1956. Measurements of fractional wettability of oilfield rocks by the nuclear magnetic relaxation method. *Transactions of the American Institute of Mining and Metallurgical Engineers* 207 (11), 262–264.
- Burdine, N.T., 1953. Relative permeability calculations from pore size distribution data. *Transactions of the American Institute of Mining and Metallurgical Engineers* 198, 71–78.

- Craig, F.F., 1971. The reservoir engineering aspects of waterflooding. Monograph Series, vol. 3. Society of Petroleum Engineers, Richardson, TX.
- Danielson, R.E., Sutherland, P.L., 1986. Porosity. Methods of soil analysis: Part 1. Physical and Mineralogical Methods. Soil Science Society of America, Madison, WI.
- Darnault, C.J.G., et al., 1998. Visualization by light transmission of oil and water contents in transient two-phase flow fields. *Journal of Contaminant Hydrology* 31 (3–4), 337–348.
- Darnault, C.J.G., 2001. Measurement of fluid contents by light transmission in transient three-phase oil–water–air systems in sand. *Water Resources Research* 37 (7), 1859–1868.
- Dawson, H.E., Roberts, P.V., 1997. Influence of viscous, gravitational, and capillary forces on dnapl saturation. *Ground Water* 35 (2), 261–269.
- Denekas, M.O., Mattax, C.C., Davis, G.T., 1959. Effects of crude oil components on rock wettability. *Transactions of the American Institute of Mining and Metallurgical Engineers* 216, 330–333.
- Donaldson, E.C., Thomas, R.D., Lorenz, P.B., 1969. Wettability determination and its effect on recovery efficiency. *Society of Petroleum Engineers Journal* 9 (1), 13.
- Hiemenz, P.C., Rajagopalan, R., 1997. Principles of colloid and surface chemistry. Marcel Dekker, New York, xix, 650 pp.
- Hofstee, C., Oostrom, M., Dane, J.H., Walker, R.C., 1998a. Infiltration and redistribution of perchloroethylene in partially saturated, stratified porous media. *Journal of Contaminant Hydrology* 34 (4), 293–313.
- Hofstee, C., Walker, R.C., Dane, J.H., 1998b. Infiltration and redistribution of perchloroethylene in stratified water-saturated porous media. *Soil Science Society of America Journal* 62, 13–22.
- Illangasekare, T.H., Ramsey Jr., J.L., Jensen, K.H., Butts, M.B. 1995. Experimental study of movement and distribution of dense organic contaminants in heterogeneous aquifers. *Journal of Contaminant Hydrology* 20 (1–2), 1–25.
- Klute, A., Dirksen, C., 1986. Hydraulic conductivity and diffusivity: laboratory methods. In: Klute, A. (Ed.), *Methods of Soil Analysis: Part I. Physical and Mineralogical Methods-Agronomy Monograph*, vol. 9. American Society of Agronomy and Soil Science Society of America, Madison, WI, pp. 687–734.
- Kueper, B.H., Redman, D., Starr, R.C., Reitsma, S., Mah, M., 1993. Field experiment to study the behavior of tetrachloroethylene below the water table. Spatial distribution of residual and pooled dnapl. *Ground Water* 31, 756–766.
- Kueper, B.H., Abbott, W., Farquhar, G., 1989. Experimental observations of multiphase flow in heterogeneous porous media. *Journal of Contaminant Hydrology* 5, 83–95.
- Lenhard, R.J., Parker, J.C., 1987. A model for hysteretic constitutive relations governing multiphase flow; 2, permeability–saturation relations. *Water Resources Research* 23 (12), 2197–2206.
- Lord, D.L., 2002. Personal communication. Sandia National Laboratories, Carlsbad, NM, USA.
- Lord, D.L., Demond, A.H., Hayes, K.F., 2000. Effects of organic base chemistry on interfacial tension, wettability, and capillary pressure in multiphase subsurface waste systems. *Transport in Porous Media* 38 (1–2), 79–92.
- Muallem, Y., 1976. A new model for predicting the hydraulic conductivity of unsaturated porous media. *Water Resources Research* 12 (3), 513–522.
- Oostrom, M., Lenhard, R.J., 1998. Comparison of relative permeability–saturation–pressure parametric models for infiltration and redistribution of a light nonaqueous-phase liquid in sandy porous media. *Advances in Water Resources* 21, 145–157.
- Oostrom, M., Hofstee, C., Walker, R.C., Dane, J.H., 1999a. Movement and remediation of trichloroethylene in a saturated heterogeneous porous medium: 1. Spill behavior and initial dissolution. *Journal of Contaminant Hydrology* 37, 159–178.
- Oostrom, M., Hofstee, C., Walker, R.C., Dane, J.H., 1999b. Movement and remediation of trichloroethylene in a saturated, heterogeneous porous medium: 2. Pump-and-treat and surfactant flushing. *Journal of Contaminant Hydrology* 37, 179–197.
- Pennell, K.D., Jin, M., Abriola, L.M., Pope, G.A., 1994. Surfactant enhanced remediation of soil columns contaminated by residual tetrachloroethylene. *Journal of Contaminant Hydrology* 16, 35–53.
- Pennell, K.D., Pope, G.A., Abriola, L.M., 1996. Influence of viscous and buoyancy forces on the mobilization of residual tetrachloroethylene during surfactant flushing. *Environmental Science and Technology* 30 (4), 1328–1335.



- Phelan, T.J., Lemke, L.D., Bradford, S.A., O'Carroll, D.M., Abriola, L.M., 2004. Influence of textural and wettability variations on predictions of DNAPL persistence and plume development in saturated porous media. *Advances in Water Resources* (in press).
- Powers, S.E., Tamblin, M.E., 1995. Wettability of porous media after exposure to synthetic gasolines. *Journal of Contaminant Hydrology* 19 (2), 105–125.
- Rathfelder, K., Abriola, L.M., 1998. Influence of capillarity in numerical modeling of organic liquid redistribution in two-phase systems. *Advances in Water Resources* 21, 159–170.
- Rathfelder, K.M., Abriola, L.M., Singletary, M.A., Pennell, K.D., 2000. Influence of interfacial tension reduction on organic liquid migration: numerical and experimental comparisons. ModelCARE '99 Conference. IAHS Publication (International Association of Hydrological Sciences), Zurich, Switzerland, pp. 439–447.
- Rathfelder, K.M., Abriola Linda, M., Singletary, M.A., Pennell, K.D., 2003. Influence of surfactant-facilitated interfacial tension reduction on chlorinated solvent migration in porous media: Observations and numerical simulation. *Journal of Contaminant Hydrology* 64 (3–4), 227–252.
- Salehzadeh, A., Demond, A.H., 1999. Pressure cell for measuring capillary pressure relationships of contaminated sands. *ASCE Journal of Environmental Engineering* 125 (4), 385–388.
- Schroth, M.H., Istok, J.D., Selker, J.S., Oostrom, M., White, M.D., 1998. Multifluid flow in bedded porous media: laboratory experiments and numerical simulations. *Advances in Water Resources* 22 (2), 169–183.
- Schwille, F., 1988. *Dense Chlorinated Solvents in Porous and Fractured Media: Model Experiments/By Friedrich Schwille* Lewis Publishers, Chelsea MI. xxx, 146 ill. (some col.) pp.
- Taylor, T.P., Pennell, K.D., Abriola, L.M., Dane, J.H., 2001. Surfactant enhanced recovery of tetrachloroethylene from a porous medium containing low permeability lenses: 1. Experimental studies. *Journal of Contaminant Hydrology* 48 (3–4), 325–350.
- Treiber, L.E., Archer, D.L., Owens, W.W., 1972. Laboratory evaluation of wettability of 50 oil-producing reservoirs. *Society of Petroleum Engineers Journal* 12 (6), 531–540.
- van Genuchten, M.T., 1980. Closed-form equation for predicting the hydraulic conductivity of unsaturated soils. *Soil Science Society of America Journal* 44, 892–898.